Association Kinetics from Single Molecule Force Spectroscopy Measurements

Senli Guo, Nimit Lad, Chad Ray, and Boris B. Akhremitchev*
Department of Chemistry, Duke University, Durham, North Carolina 27708

ABSTRACT Single molecule force spectroscopy is often used to study the dissociation of single molecules by applying mechanical force to the intermolecular bond. These measurements provide the kinetic parameters of dissociation. We present what to our knowledge is a new atomic force microscopy-based approach to obtain the activation energy of the association reaction and approximate grafting density of reactive receptors using the dependence of the probability to form molecular bonds on probe velocity when one of the interacting molecules is tethered by a flexible polymeric linker to the atomic force microscopy probe. Possible errors in the activation energy measured with this approach are considered and resulting corrections are included in the data analysis. This new approach uses the same experimental setup as traditional force spectroscopy measurements that quantify dissociation kinetics. We apply the developed methodology to measure the activation energy of biotin-streptavidin association (including a contribution from the steric factor) and obtain a value of 8 $\pm$ 1 kT. This value is consistent with the association rate measured previously in solution. Comparison with the solution-derived activation energy indicates that kinetics of biotin-streptavidin binding is mainly controlled by the reaction step.

INTRODUCTION

Single-molecule force spectroscopy measures unbinding kinetics at a single molecule level and has been used widely to study very different classes of interactions: from specific interactions between biomolecules to nonspecific hydrophobic interactions (1–3). However, the associative part of bimolecular reactions has been rarely investigated. There are two force spectroscopy approaches to characterize kinetic parameters of association; both of these approaches are based on atomic force microscopy (AFM) measurements (4,5). The method by Friddle et al. (4) analyzes rupture forces between molecules immobilized on the substrate and on the AFM probe and uses the statistical models of rebinding kinetics to obtain the activation energy of association. To obtain a measurable effect of rebinding, this method requires direct tetherless attachment of molecules to the cantilever probes. Such attachment abandons benefits of using polymeric tethers and does not discriminate against nonspecific binding events (6,7). Moreover, using this approach requires independent knowledge of the grafting density of molecules to substrates. In the second approach by Hinterdorfer et al. (5) the rate of association is quantified by assuming that the tethered ligand always probes the constant volume. This method gives reasonable values of association rate constants when short tethers are used (8 nm long poly(ethylene glycol)) (5,8). However, using longer tethers is beneficial in facilitating single-molecule detection and in reduction of noise (6). It is known that the probability to react between tethered ligand and receptor depends on waiting time and for longer tethers this time dependence becomes experimentally relevant (9). Therefore the expected tether dynamics effects might be exploited to characterize kinetics of association and promote comparison with solution experiments.

In this study, we describe an experimental approach that uses the AFM-based single-molecule force spectroscopy approach. In this approach kinetics of binding and dissociation can be measured simultaneously. The dissociation part of these measurements has been considered in detail recently (10). A theoretical model of binding kinetics in experiments that use tethered ligands is described. Polymer dynamics models are used to determine the relationship between the probability of binding and the activation energy of association of a partially diffusion-controlled bimolecular reaction. The developed model is applied to experimental measurements of binding kinetics between biotin and streptavidin molecules. This receptor-ligand pair is selected for studies here because the bond rupture occurs at significant force (~50–100 pN) facilitating accurate measurements of binding probabilities (10). This strong interaction has been researched thoroughly in experiments and simulations (1,10–16).

This study contains both theoretical and experimental parts. In the theoretical section, binding probability is derived for two polymeric tether models: the freely jointed chain model and the Gaussian chain model. The simpler Gaussian tether model is used for evaluation of various factors affecting accuracy of the measured activation energy and to describe how the expected systematic errors might be avoided and/or corrected. The expected outcomes of this single-molecule approach are then compared with kinetics from solution-based surface plasmon resonance (SPR) measurements. Finally, the developed model is applied to analyze binding probability between tethered biotin ligand and streptavidin receptor. In two separate experiments biotin was tethered using tethers of different length. Activation

Submitted October 6, 2008, and accepted for publication January 22, 2009.

*Correspondence: boris.a@duke.edu

Editor: Gerhard Hummer.

0006-3495/09/04/3412/11 $2.00

doi: 10.1016/j.bpj.2009.01.031

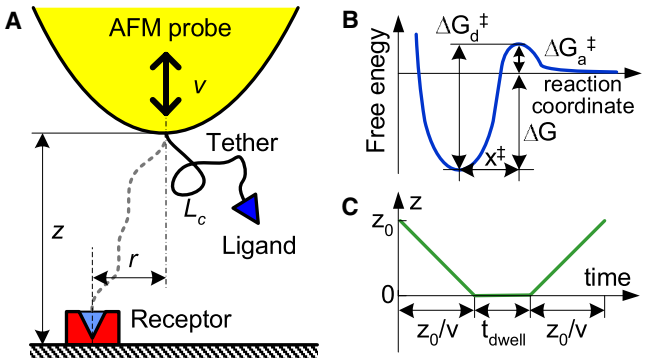

FIGURE 1 Cartoons of (*A*) experimental setup and (*B*) the ligand-receptor potential of mean force. (*C*) Probe-sample separation during one cycle of probe reciprocating motion.

energy of association and approximate surface coverage are extracted from statistics of rupture data. The measured activation energy is then compared to kinetics of association measured previously and is found to be reasonably accurate.

THEORETICAL MODEL

General model

To develop a model for associative binding reactions we consider AFM experiments that measure rupture forces between a ligand tethered to the AFM probe and a surface-bound receptor. (This might also represent a model for recognition of a tethered ligand by a cell receptor and cell adhesion.) Efficiency of binding depends on two factors: the probability of molecules to encounter each other and the rate of the binding step (17–20). In experiments the probe undergoes a reciprocating up-down motion and the ligand can bind to a receptor during the probe approach, withdrawal, or during the time the probe dwells on the substrate as illustrated in Fig. 1. For binding to occur, the tether should be extended enough to bridge the probe and the receptor. For a tether covalently attached at the apex of the AFM probe and with low grafting density of receptors the probability to form a bond is (9):

$$p(r) = 1 - \exp\left[-\left(k(r)t_{\mathrm{dwell}} + 2\int_0^{z_0/v} \mathrm{d}\tau k(d(\tau))\right)\right], \quad (1)$$

where the exponential term gives the survival probability of unbound ligand, $k(r)$ is the distance-dependent rate of the receptor-ligand bonding, d is the end-to-end distance of the tether when the tether bridges the tip and the receptor, τ is time of up-down probe motion, r is the displacement of the receptor from the projection of the fixed tether end onto the substrate (Fig. 1 *A*), and t_{dwell} is the dwell time the probe spends in contact with the surface, z_0 is the maximum probe distance from the substrate where the receptor-ligand binding remains thermodynamically favorable and v is the probe velocity. The factor of two under the exponent is included to consider the up and down motion of the probe.

If the grafting density θ of receptors on the substrate is low then the probability to form a bond during one approach-withdraw cycle can be calculated by integrating the probability given by Eq. 1:

$$P = 2\pi\theta\int_0^{\infty} p(r)r\mathrm{d}r. \quad (2)$$

For a fixed probe and receptor geometry (similar to that shown in Fig. 1 *A*) the rate of bond formation depends on the probe position z and can be calculated as

$$k(d) = A\exp\left[-\left(\Delta G_a^{\ddagger} + G_t(d)\right)/k_BT\right], \quad (3)$$

where G_t is the free energy of the stretched tether, A is the receptor-ligand encounter rate when $G_t = 0$, $\Delta G_a^{\ddagger}$ is the activation energy (as illustrated in Fig. 1 *B*) and k_BT is the thermal energy. Free energy of the stretched tether can be calculated by using different physical models of polymers by noting that the end-to-end distance of the tether is given by $d = ((z_0 - v\,t)^2 + r^2)^{1/2}$. Therefore, for specified parameters of v, t_{dwell}, $\Delta G_a^{\ddagger}$, θ, and z_0 and using a particular model of polymer stretching to calculate G_t and a model of relative diffusion of the tether ends to calculate the receptor-ligand encounter rate A the binding probability during the approach-withdraw cycle can be calculated numerically. However, this numerical calculation requires double integration in Eqs. 1 and 2 and therefore is not efficient. Below we consider approximate models that provide physical insight into the binding probability dependence on experimental parameters and can be used to extract the unknown values of parameters by measuring the binding probability.

Calculations of the radial binding probability $p(r)$ and the total binding probability P calculated by the exact Eqs. 1 and 2 are shown in Figs. 2 and 3, respectively. Parameters used in these calculations are close to parameters of typical AFM experiments. The encounter rate used in these figures is calculated according to the modified SSS model as explained below. It can be noted that for longer chains the difference between binding distance detected with and without waiting becomes evident and therefore should be included in the analysis of binding probability. The dependencies shown in Fig. 3 indicate that in measurements with nonzero dwell time the measurable velocity dependence of the binding probability might be confined to the region of impractical low velocities and therefore difficult to detect.

Approximate model of radial binding probability

As illustrated in the inset in Fig. 2, the radial probability to form a bond given by Eq. 1 as a function of the receptor displacement r can be approximated as a step function. Therefore, the binding probability can be approximated by $P = \pi\,\theta\,\tilde{r}^2$ where $\tilde{r}$ is a displacement at which the radial

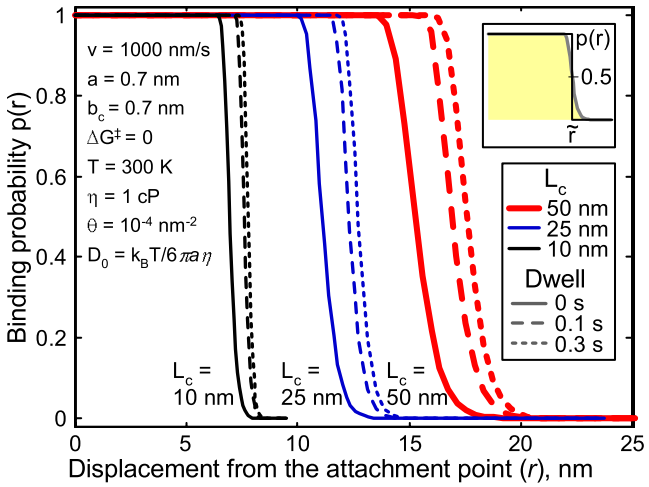

FIGURE 2 Radial distribution of binding probability for FJC tethers of different lengths. Calculation parameters are shown in the figure.

distribution $p(r)$ decreases to 1/2. From Eq. 1 we obtain the following equation for $\tilde{r}$:

$$\frac{\ln 2}{\tilde{A}} = t_{\text{dwell}} e^{-\frac{G_t(\tilde{r})}{k_B T}} + 2\int_0^{z_0/v} d\tau e^{-\frac{G_t\left(\sqrt{(z_0 - v\tau)^2 + \tilde{r}^2}\right)}{k_B T}}. \quad (4)$$

Here the activation barrier $\Delta G_a^{\ddagger}$ is included in the factor of the effective encounter rate $\tilde{A} = A\exp(-\Delta G_a^{\ddagger}/k_B T)$. Solution of Eq. 4 to find $\tilde{r}$ depends on the tether model. Below we derive solutions for two polymeric tether models: the Gaussian tether model and the freely jointed chain (FJC) model. A simple solution using the worm-like chain (WLC) model could not be found. We note that the polymer we use in our experimental work is rather flexible (monomer size ~0.36 nm, Kuhn length ~0.7 nm) (21). Therefore it does not satisfy the underlying assumption of the WLC model that change in the polymer backbone direction between the adjacent monomers is small. However, using the WLC model would be appropriate in experiments that use double-stranded DNA as a tether (22).

Gaussian tether model

The free energy of the stretched tether as a function of the end-to-end distance d is given by $G_t = 3/2k_B T d^2/\tilde{l}^2$ where $\tilde{l}$ is the root mean-square (RMS) end-to-end distance of the unperturbed chain $\tilde{l} = \sqrt{a L_c}$, a is the Kuhn length and L_c is the contour length. The solution of Eq. 4 is then given by

$$\tilde{r} = \tilde{l}\sqrt{2/3}\ln^{\frac{1}{2}}\left(\frac{\tilde{A}}{\ln 2}\left[t_{\text{dwell}} + \frac{\tilde{l}\sqrt{2\pi/3}}{v}\text{erf}\left(\frac{z_0}{\tilde{l}\sqrt{2/3}}\right)\right]\right). \quad (5)$$

A simplification of the error-function factor in Eq. 5 is possible. The ligand-receptor bond will be thermodynamically stable only if $3/2k_B T\, z_0^2/\tilde{l}^2 \le \Delta G$ where ΔG is the thermodynamic energy difference between the free and the bound ligand (Fig. 1 *B*). This gives maximum $z_0 = \tilde{l}\sqrt{2\Delta G/3k_B T}$. On the other hand, in the proposed detection method, the binding is detected by measuring rupture forces. The detected rupture force should noticeably exceed the noise of the AFM instrument (~1–10 pN) and for typical experimental conditions this implies that the thermodynamic energy difference should exceed ~10 $k_B T$. Consequently the error function factor is different from unity by ~10^{-6} and can be safely replaced with a factor of 1. The resulting equation for binding probability simplifies to

$$P = \frac{2\pi}{3}\theta\tilde{l}^2\ln\left(\frac{\tilde{A}}{\ln 2}\left[t_{\text{dwell}} + \frac{\tilde{l}\sqrt{2\pi/3}}{v}\right]\right). \quad (6)$$

In the limit of very low binding probability Eq. 6 predicts that the binding probability scales linearly with the characteristic experimental time similar to the result obtained previously based on surface force apparatus measurements (9). It should be noticed that Eq. 2 (and consequently Eq. 6) does not predict correctly the binding probability when the probability approaches unity.

In typical AFM experiments the probe motion toward the surface continues until a typical threshold deflection δ of the cantilever is reached (the deflection trigger). Therefore for hard surfaces the surface dwell time can be written as $t_{\text{dwell}} = t_0 + 2\delta/v$ where t_0 is the intentional dwell time that the probe spends on the surface. (For soft surfaces the deflection trigger δ should be replaced with the probe travel z between the contact point and the deflection trigger event. It should be noted that if the elasticity of the surface is inhomogeneous the resulting variation in the contact area between the probe and the surface might additionally affect the binding probability. However, detailed consideration of this aspect is beyond the scope of this study.) In typical experiments $\delta \approx 5$ nm and $\tilde{l} \approx 5$ nm; consequently to observe the velocity dependence of rupture probability the intentional dwell time t_0

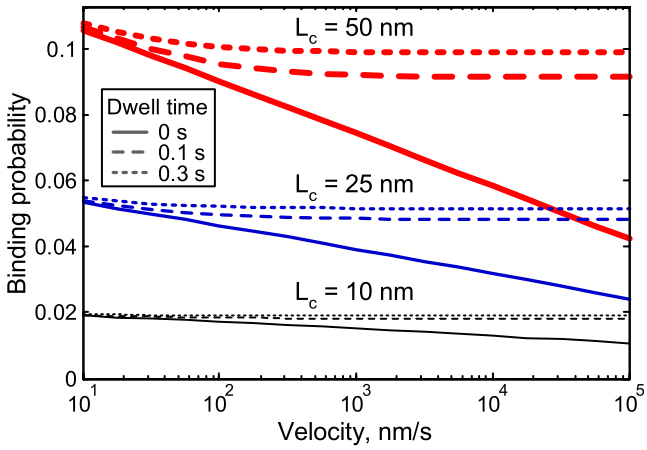

FIGURE 3 Binding probability as a function of probe velocity. Calculation parameters are identical to parameters used in Fig. 2.

should be small (for typical $v = 1000$ nm/s the t_0 time should be <10 ms). For $t_0 = 0$ Eq. 6 predicts that

$$\frac{dP}{d\ln(v)} = -2\pi\theta\tilde{l}^2/3. \quad (7)$$

This means that with the Gaussian chain model the binding probability versus probe velocity is linear in the semi-log coordinates and the slope of this line depends only on the receptor surface coverage, and the tether RMS length. Equation 7 also indicates that for experiments with short tethers the dependence of binding probability on probe velocity might be hidden by statistical uncertainty of the rupture events detection.

Additional analysis of Eq. 6 clarifies some of the limitations of the proposed method. Binding probability is positive; this requires that $\Delta G_a^{\ddagger}/k_BT < \ln(A\tilde{l}\sqrt{2\pi/3}/(v\ln 2))$ for the step-function representation of the radial binding probability to be valid (for $t_{dwell} = 0$). This gives the upper limit of the activation energy where the Gaussian chain model can be applied. On the other hand, $P < 1$ therefore Eq. 6 limits the surface coverage that can be used in experiments to $\theta < (2\pi\tilde{l}^2\ln[\tilde{A}\tilde{l}\sqrt{2\pi/3}/(v\ln 2)]/3)^{-1}$.

FJC tether model

Free energy of the stretched tether can be calculated using the FJC model as

$$G_t(d) = k_BTN_K\int_0^{d/L_c} L^{-1}(x)dx \approx k_BTN_K\left[\frac{d(3dL_c - 3L_c^2 - d^2)}{3L_c^3} - \ln\left(1 - \frac{d}{L_c}\right)\right], \quad (8)$$

where d is the end-to-end distance of the tether stretched to make the receptor-ligand bond, N_K is the number of Kuhn segments in the tether, and L^{-1} is the inverse Langevin function ($L(x) = \coth(x) - 1/x$). (To integrate Eq. 2 the inverse Langevin function was approximated by $L^{-1} = 1/(1 - x) - (1 - x)^2$. This approximation of L^{-1} has maximum error of 2.6% in the interval $0 < x < 1$).

To calculate the integral in Eq. 4 using Eq. 8 it is convenient to write $\tilde{r} = L_c\ y$. Then Eq. 4 can be solved approximately with a recursive equation for y (using the first order Taylor expansion polynomial of d at $r = 0$ or at $\tau = z_0/v$):

$$y = 1 - \left(\frac{\ln 2}{\tilde{A}}\left[\frac{16a}{v}(1 - y) + t_{dwell}\right]^{-1}\right)^{1/N_K} \times \exp[-y(1 - y + y^2/3)] \quad . \quad (9)$$

Numerical computations show that recursive calculations using Eq. 9 with an initial guess of $y = 0$ converge to 10^{-6} tolerance within ~15 steps for the range of probe velocities from 10 to 10^5 nm/s and parameters typical for AFM experiments. With y calculated by Eq. 9 the binding probability is $P = \pi\theta L_c^2y^2$. In experiments with $t_0 = 0$ and long tethers the FJC model gives the same scaling of the probability with the logarithm of the probe velocity as the Gaussian tether model. It can be shown that under these conditions $dP/d\ln(v) \approx -2\pi\theta L_c\ a/3$. This relation can be used for approximate estimation of the surface coverage θ.

Equation 9 gives the limit of applicability of the step-function approximation of $p(r)$ with the FJC tether model. By setting $y = 0$ in Eq. 9 the minimum effective encounter rate is

$$\tilde{A}_{min} = \ln 2(16a/v + t_{dwell})^{-1}. \quad (10)$$

This indicates that for a typical range of probe velocities the proposed approach will fail for long tethers and high activation barriers because both lower the factor $\tilde{A}$. It is interesting to compare this result with the result for the Gaussian tether. Taking $t_{dwell} = 0$ then $\tilde{A}_{min}^{FJC}/\tilde{A}_{min}^{Gauss} \approx \sqrt{N_K}/11$, showing that for typical PEG tethers used in our AFM measurements ($N_K \approx$ 40–70) both models have similar value of the maximum activation energy that can be measured by this approach.

Encounter rate

The encounter rate prefactor A can be estimated using the polymer loop formation theory of Szabo, Schulten, and Schulten (17) (SSS model) as

$$A_{SSS} = 3\sqrt{6/\pi}D_0b_c/\left(N_K^{3/2}\,a^3\right), \quad (11)$$

where b_c is the capture distance, D_0 is the ligand diffusion coefficient, and a is the Kuhn length. It should be noted that using the polymer loop formation model to calculate the encounter rate leads to incorporation of the steric factor into the extracted activation energy (19,23,24). Therefore the activation energy extracted with this model might differ from results of the temperature-dependent measurements. Further discussion of this subject is continued below in the subsection considering uncertainties in the measured parameters and in relation to experimental results.

For small ligands, the diffusion coefficient is taken as the diffusion coefficient of a sphere with radius equal to the Kuhn length: $D_0 = k_BT(6\pi a\eta)^{-1}$, where η is the viscosity of solution (25). The capture distance corresponds to the distance at which the ligand is captured by the receptor. It was pointed out that for the loop formation of a freely-jointed chain the minimum physically meaningful capture length equals to the Kuhn length (25). However, setting $b_c = a$ might result in a systematic error in the estimation of activation energy: change in the capture distance by a factor of 2 changes the activation energy $\Delta G_a^{\ddagger}$ by ~0.7 k_BT. For biotin-streptavidin bond formation the capture distance is likely to be close to the distance between the equilibrium state and the transition state $x^{\ddagger}$. The simulated potential of mean force of biotin-avidin interaction has an inner barrier at ~0.55 nm and an outer barrier at ~1.2 nm (1). Therefore by keeping $b_c = 0.7$ nm the resulting error in the activation energy is unlikely to exceed 0.5 k_BT. We add this 0.5 k_BT contribution to the random error of the activation energy in our data analysis.

It was noted that Eq. 11 disagrees with the simulation results and incorrectly predicts scaling of the first passage time (25). Modified SSS theory gives a different prediction of the encounter rate (25):

$$A_c = 24\sqrt{6}\, D_0 b_c / \left(\pi N_K^2 a^3\right). \quad (12)$$

It can be noted that the ratio $A_{SSS}/A_c = \sqrt{\pi N_K}/8$ is a factor of ~1.6 for polymers with length similar to the length of tethers used in the experimental part of this study. For polymers of such length and with the capture length equal to the Kuhn length simulations show that the SSS model overestimates the loop formation rate by a factor of ~3 (26). Therefore, selection of a particular encounter rate model adds uncertainty to the activation energy. Consequently in the data analysis below we use the modified SSS model and add a 0.5 k_BT contribution to the random error of the activation energy.

Substituting Eq. 12 and the Einstein-Stokes diffusion coefficient into the Gaussian tether model Eq. 6 gives

$$P = \frac{2\pi}{3}\theta\tilde{l}^2\left(-\frac{\Delta G_a^{\ddagger}}{k_BT} + \ln\left[\frac{4\sqrt{6}}{\pi^2 \ln 2}\frac{k_BTb_c}{\tilde{l}^2\eta}\left(t_0 + \frac{2\delta + \tilde{l}\sqrt{2\pi/3}}{v}\right)\right]\right). \quad (13)$$

Equation 13 predicts that the binding probability depends on the unperturbed RMS tether size $\tilde{l}$ and does not include explicit dependence on the Kuhn or contour lengths. This means that binding probability with short stiff tethers will be the same as with long flexible tethers if $\tilde{l}$ is the same in both cases. Because this conclusion is based on the Gaussian chain model, it is expected that in experiments with short tethers and large ligands this scaling is not accurate. Also, in this form of binding probability dependence on velocity, it becomes more clear how the surface coverage can be separated from the activation energy: the surface coverage contributes to the slope and the intercept of P versus $\ln(v)$ dependence (at small t_0) whereas the activation energy contributes only to the intercept of this dependence.

Uncertainty in the measured parameters

In this section we consider several effects that might affect the accuracy of the measured activation energy. First we consider various contributions to the error of parameters for experiments with the tethered ligand and then also consider deviation of the activation energy measured by the method proposed here from the measurements in solution. We note that some effects merely mentioned in this section require more detailed consideration elsewhere.

Effects of tether polydispersity, uncertainty in the capture length, and multiple bond ruptures

For experiments with $t_0 = 0$ Eq. 13 can be written to show how the activation energy can be measured from a set of experiments carried out at different probe velocities:

$$\frac{\Delta G_a^{\ddagger}}{k_BT} = \left\langle \ln\left[\frac{4\sqrt{6}k_BTb_c}{\pi^2\ln 2}\frac{\left(2\delta + \tilde{l}\sqrt{2\pi/3}\right)}{\tilde{l}^2\eta v}\right] + \frac{P(v)}{\overline{dP/d\ln v}}\right\rangle. \quad (14)$$

On the right-hand side of Eq. 14 $\overline{dP/d\ln v}$ is the slope of the binding probability dependence on the logarithm of the probe velocity and the angular bracket indicates averaging over all velocities. Equation 14 shows how the uncertainty in experimental parameters affects the extracted activation energy. For example, 50% uncertainty in the capture length b_c results in ~1/2 k_BT error in the activation energy; also, 50% uncertainty in the tether contour length results in error between 1/4 and 1/2 k_BT, depending on the relative value of the deflection trigger δ with respect to $\tilde{l}$.

However, this assumes that only one molecule is attached to the AFM probe. In real experiments it is likely that the number of grafted molecules is more than one. In this case a single detected rupture event might correspond to the simultaneous rupture of more than one molecular bond (10,27–29). Therefore the grafting density extracted from experiments might noticeably differ from the true grafting density of the reactive receptors.

Off-apex attachment of the tether

Another assumption used in the theory above is that the tether is attached at the apex of the AFM tip. However, some offset from the apex might occur in practice. Using the Gaussian tether model for simplicity, the binding probability that considers the offset of the attachment point from the tip apex by z_{off} is

$$P = \frac{2\pi}{3}\theta\tilde{l}^2\ln\left(\frac{\tilde{A}}{\ln 2}\left[t_{dwell}\exp\left(-\frac{3z_{off}^2}{2\tilde{l}^2}\right) + \frac{\tilde{l}\sqrt{2\pi/3}}{v}\left(\mathrm{erfc}\,\frac{z_{off}}{\tilde{l}\sqrt{2/3}}\right)\right]\right), \quad (15)$$

where erfc is the complimentary error function. Then Eqs. 14 and 15 can be used to estimate the systematic error in the activation energy due to the off-apex tether attachment. The resulting error is:

$$\Delta\Delta G_a^{\ddagger}/k_BT = \ln\left(\mathrm{erfc}\left[\sqrt{3/2}\, z_{off}/\tilde{l}\right]\right). \quad (16)$$

In actual experiments the place of the tether attachment is unknown, however, an average systematic error can be calculated assuming that tethers can uniformly attach to the AFM probe. From Eqs. 15 and 16 the average systematic error is

$$\left\langle \Delta\Delta G_{\mathrm{a}}^{\ddagger} \right\rangle = \frac{\int_0^{z_{\mathrm{off,max}}} \Delta\Delta G_{\mathrm{a}}^{\ddagger}\left(z_{\mathrm{off}}\right) P\left(z_{\mathrm{off}}\right) \mathrm{d}S}{\int_0^{z_{\mathrm{off,max}}} P\left(z_{\mathrm{off}}\right) \mathrm{d}S}. \qquad (17)$$

Here $\Delta\Delta G_{\mathrm{a}}^{\ddagger}(z_{\mathrm{off}})$ is given by Eq. 16, $P(z_{\mathrm{off}})$ is given by Eq. 15 and dS is the surface area of the probe located at height z_{off} from the apex, $z_{\mathrm{off,max}}$ is the maximum offset of the tether attachment point were the binding probability computed by Eq. 15 becomes zero. For an AFM probe with paraboloidal shape and tip radius of curvature R the surface area $\mathrm{d}S = 2\pi\sqrt{R\ (R + z_{\mathrm{off}})}\ \mathrm{d}z_{\mathrm{off}}$. Therefore the average systematic error can be computed numerically using Eqs. 15–17. Numerical calculations show that overestimation of the activation energy decreases with an increase of the tip radius R. However, for R in the range from 5 to 100 nm this dependence is weak (in this range the energy overestimation error decreases by ~15%) and therefore in the following estimates we use $R = 30$ nm. An average overestimation of the activation energy strongly depends on the activation energy itself as shown in Fig. 4. The correct activation energy is plotted against the expected outcome of the measurements for three different probe velocities. It can be noticed that the systematic error decreases with an increase of the activation energy. A substantial activation energy (~3 $k_{\mathrm{B}}T$) is expected to be measured even for barrierless reactions. Uncertainty of the tether attachment point is a significant contribution to the systematic error. However, because FJC tethers extend to shorter distances than Gaussian tethers, the systematic error estimated above is the upper bound of the systematic error for realistic tethers.

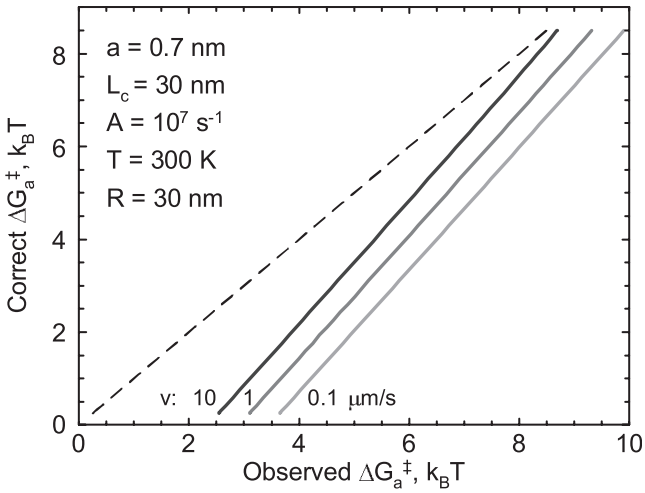

FIGURE 4 Correct versus the expected activation energy. Calculation parameters are shown in the figure. Dashed line corresponds to the correct activation energy.

Uncertainty in detection probability of rupture events

The detection of binding events occurs by identifying the rupture events in the measured force plots. In the measurements presented here the rupture forces are high (typically >50 pN) and therefore detection occurs with nearly 100% efficiency. However, for other molecular systems rupture forces of interactions between single molecules might be noticeably lower (30–32). Therefore, we briefly consider possible effects of noise on the measured parameters. The cantilever RMS noise is given by (33,34)

$$F_{\mathrm{noise}} = \left[B\left(\frac{4k_{\mathrm{B}}T\kappa_{\mathrm{c}}}{\omega_0 Q} + \Delta F_{\mathrm{white}}^2 \right) + \Delta F_{\mathrm{DC}}^2 \right]^{1/2}. \qquad (18)$$

Here κ_{c} is the cantilever spring constant, B is the detection bandwidth, ω_0 is the angular resonant frequency of the cantilever and Q is the quality factor, $\Delta F_{\mathrm{white}}$ is the white noise, and ΔF_{DC} is the DC noise. The rupture forces of molecular bonds are stochastic values with a nonsymmetric distribution around the most probable value (35). At some cantilever velocities a portion of the expected rupture forces might be below the detection limit given by Eq. 18. As discussed earlier, this might occur at low as well as at high cantilever velocities (10). Therefore the detection probability dependence on velocity will change from the prediction given by Eq. 2. This might be manifested by noticeable changes in the slope in P versus ln(v) coordinates. In this case the force noise should be compared with the distribution of rupture forces to avoid artifacts in interpreting the binding probability dependence on velocity. In addition, we note that for the accurate measurements of the activation energy of dissociation the apparent loading rate should be determined and therefore the signal-to-noise ratio required in such measurements should be noticeably higher than 1 (we typically use signal-to-noise ratio of 4 in computer-aided identification of the rupture events that are consequently used in the analysis of forced dissociation). In contrast, method of measuring activation energy of association proposed here requires only the detection of the rupture events and therefore is more tolerant to the force noise permitting studying of molecular bonds that cannot be accurately quantified by the standard force spectroscopy experiments.

Another factor that might affect the detected binding probability are the rupture events from nonspecific interactions (36). Separate control experiments should be carried out to ensure that the detected rupture events correspond to the interaction understudy (37). If nonspecific binding events contribute significantly to the detected rupture probability the extracted activation energy will have no physical meaning.

Comparison to experiments in solution

It was noticed previously in relation to SPR experiments that immobilization of molecules might affect the measured

kinetics (38). It was proposed that using different immobilization chemistry might help to characterize possible effects of immobilization such as conformational changes and steric restrictions of access to the binding sites (38). Using polymeric tethers to attach both binding partners might additionally affect the association kinetics because of the tether interfering with binding at the binding site and changes in the translational and rotational diffusion of the ligand (23). If interference of immobilization with the binding site is significant then no specific rupture events will be detected, particularly considering the limited force sensitivity of AFM instruments. In experiments described here, biotin is attached through the carboxyl group of valeric acid that in the bound state is located near the exit from the binding pocket (39). Therefore no significant steric effects are expected from the tether attachment. On the other hand, tethering of a small ligand by a rigid linker might significantly reduce the diffusion coefficients. Here we note that the Kuhn length of polymeric tethers used in this experiments is similar to the size of biotin molecule. This observation suggests that restrictions on the diffusion of biotin imposed by the tether are unlikely to be a major factor contributing to the measured activation energy. The Results and Discussion section below includes more qualitative discussion of the tethering effects in relation to experiments reported here. Other potential artifacts of SPR measurements include effects of the steric hindrance, spatial inhomogeneities, and mass-transport limitations (38). The AFM-based approach described here uses low grafting density thus reducing these effects. Ligands in the AFM approach are brought to the surface directly, eliminating the mass-transport limitations of SPR and other biosensor techniques that rely on diffusion of reactants to the sensor surface (40). Therefore, kinetic results obtained with AFM might differ from the kinetics measured with biosensors that are expected to underestimate rates of association (38).

MATERIALS AND METHODS

Sample preparation

Samples were prepared using methods reported previously (10) with slight modification as indicated below. All chemicals were purchased from Sigma-Aldrich (St. Louis, MO), unless indicated otherwise. Briefly, silicon nitride AFM probes (Veeco (Santa Barbara, CA), model NP) and glass microscope coverslips (Fisher Scientific, Hampton, NH) were cleaned in 2% Hellmanex II (Hellma GmbH & Co KG, Müllheim, Germany) aqueous solution for 3 h. Next, the probes and substrates were rinsed with deionized water (18 MΩ × cm), followed by anhydrous ethanol, then dried under vacuum for 12 h, and transferred into a nitrogen-filled glove box. The probes and substrates were aminated in a saturated ethanolamine hydrochloride solution in anhydrous DMSO for 72 h at room temperature. α-*N*-hydroxy-succinimide-ω-maleimide-poly(ethylene glycol)-biotin (NHS-PEG-biotin) linkers with a mass-average molecular mass of 3400 Da and 5000 Da (Laysan Bio, Arab, AL) were covalently attached to the aminated probes through an NHS-amine reaction in two separate experiments. This reaction was carried out for 24 h in anhydrous dimethyl formamide (DMF) with 10% pyridine (v/v). Acetic anhydride, pyridine, and DMF mixture solution (v/v, 3:4:5) was added for overnight incubation to block the remaining amines. The probes were then immersed in preheated hexanes/*i*-propanol (3:2) for 1 h. Next, the probes were cleaned successively in toluene, DMF, and ethanol for 30 min each with a platform shaker. Finally the probes were dried in vacuum and used immediately for data collection. The aminated substrates were first activated to bind amines with a solution of 10 mg of 1,4-phenylenediisothiocyanate in 200 μl DMF with 10% pyridine (v/v) for 2 h. The substrates were cleaned by ultrasonication in DMF and ethanol twice for 2 min each. Then 200 μl of 100 μg/ml solution of streptavidin in phosphate buffer (PBS; VWR International, West Chester, PA; 0.1 M pH 7 and pH 10 PBS were mixed together to reach pH 8) was deposited on the 1,4-phenylenediisothiocyanate-activated substrates. The covalent attachment of streptavidin was carried out in a dark environment for 3 h. Finally, the substrates were thoroughly rinsed with pH 7 PBS solution and used immediately for data collection.

Data collection and analysis

Data collection procedures were similar to those reported previously (10). Force spectroscopy experiments were carried out using an Asylum Research (Santa Barbara, CA) MFP-3D AFM. All measurements were carried out in 0.1 M pH 7 PBS at 25°C. A custom-made temperature stage was used to set the temperature and a custom-made O-ring was used to reduce evaporation of the PBS when the AFM probe was engaged over the sample. Force curves were collected during the reciprocating probe motion toward and away from the substrate. Simultaneously with the force curve collection, the probe was raster scanned over a 5×5 μm^2 square area on the substrate (force-volumes with 32×32 lateral size) to obtain a good statistical average. A total of 4096 force curves were collected in a series of measurements carried out at each given probe velocity with 0.2 s surface dwell time and then 10,240 force curves were collected without probe dwell on the surface. The 500 pN relative trigger (corresponding to deflection δ of ~8 nm) was used for all measurements. During collection of force curves, the probe velocity was cycled from high to low value and back several times to distribute possible effects of the probe mechanical wear over the data collected at different velocities.

Data analysis procedures were also similar to those reported previously (10). Filters with a threshold of four RMS noise value and the single tether's stretched lengths (10–50 nm for 3400 Da PEG; 15–70 nm for 5000 Da PEG) were used to automatically choose the force curves that had the potential to be considered as rupture events.

RESULTS AND DISCUSSION

Comparison of two tether models

Fig. 5 compares the binding probability dependence on probe velocity for the exact model using FJC tethers, the approximate model for FJC tethers calculated using Eq. 9, and the Gaussian tether model calculated using Eq. 6. Calculation parameters are included in the Fig. 5 legend. As can be noted, the approximate FJC model is more accurate for short tethers whereas the Gaussian tether model is more accurate for long tethers. The Gaussian tether model noticeably overestimates probability of large extension for short chains on the timescale of measurements and therefore we use the approximate FJC-based model in our data analysis. It can be noted that the Gaussian tether model is reasonably close to the exact solution justifying the use of this model in the analysis of errors presented above.

It might be expected that deviations in the binding probability calculated by the approximate models from the exact model will result in an error in the measured activation

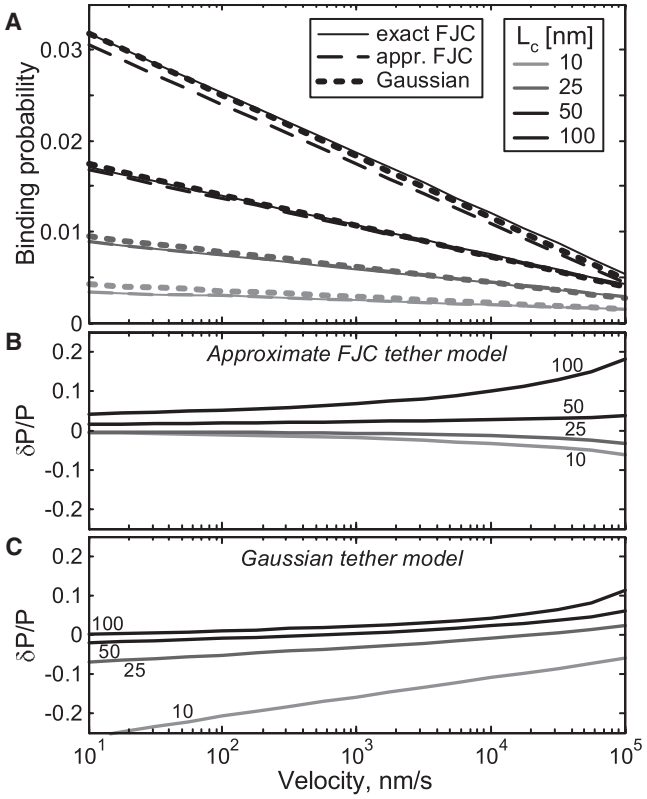

FIGURE 5 (*A*) Binding probability calculated for tethers of different length using the FJC model according to exact Eq. 1, approximate FJC model Eq. 8 and approximate Gaussian tether model Eq. 6. Calculation parameters are $t_{dwell} = 0$ s, $a = 0.7$ nm, $\Delta G_a^{\ddagger} = 3\ k_BT$, $T = 300$ K, $\eta = 1$ cP, and $\theta = 2\ 10^{-5}$ nm^{-2}. (*B* and *C*) Difference between the exact FJC and approximate FJC and Gaussian tether models, respectively.

energy. To obtain quantitative measure of these errors binding probability dependencies were calculated by the exact model for the practical range of probe velocities (10^2–10^4 nm/s) and the resulting velocity dependencies were fit by the approximate models. This comparison indicated that the approximate models underestimate the true activation energy and might even give a negative activation energy as shown in Fig. 6. The Gaussian tether model gives substantial errors ($>k_BT$) for low activation barriers and short tethers. The approximate FJC-based model performs significantly better with error noticeably below thermal energy for the wide parameter range. The noticeable upturn in the error for long tethers and high activation energies is a consequence of a limited applicability of this data analysis approach as discussed above (Eq. 10). This comparison indicates that when analyzing experimental data with unknown activation energy using the Gaussian tether model might result in very significant error and therefore it is more appropriate to use an approximate FJC-based model Eq. 9. In addition we note that factor ln(2) in equations above is somewhat arbitrary and replacing it with 1/2 reduces the model errors shown in Fig. 6 by ~0.3 k_BT thus decreasing the absolute error of the FJC-based model to below ~0.3 k_BT.

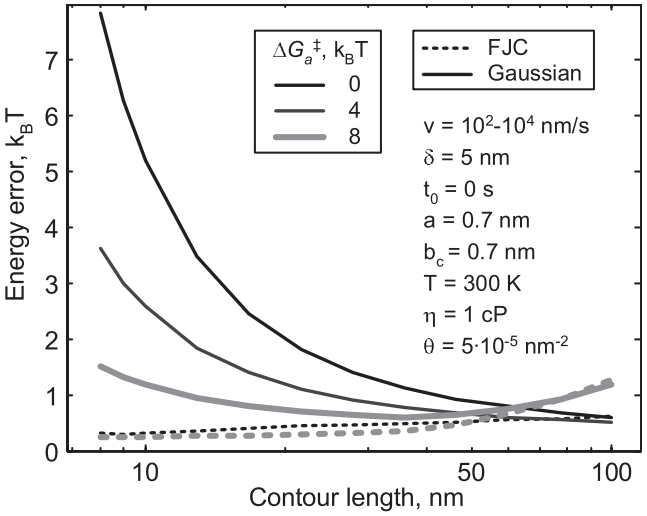

FIGURE 6 Expected error in the activation energy resulting from application of approximate theories calculated for tethers of different length. Other calculation parameters are shown in the figure.

Detection of rupture forces

Three typical force curves and one fit by the eFJC model are shown in Fig. 7. The force curves successfully fit by the eFJC model were kept as the final force curves corresponding to the rupture events for extracting kinetic parameters. These force curves were counted providing the binding probability for each probe velocity used in experiments. We note that measurements of the activation energy of association do not require quantitative measurements of the rupture forces and loading rates. Fitting of eFJC model to the data were used here to aid an automated data analysis and distinguish molecular dissociation events from spikes of noise in the force plot. The subsequent data analysis was carried out using custom software written for MATLAB (The MathWorks, Natick, MA).

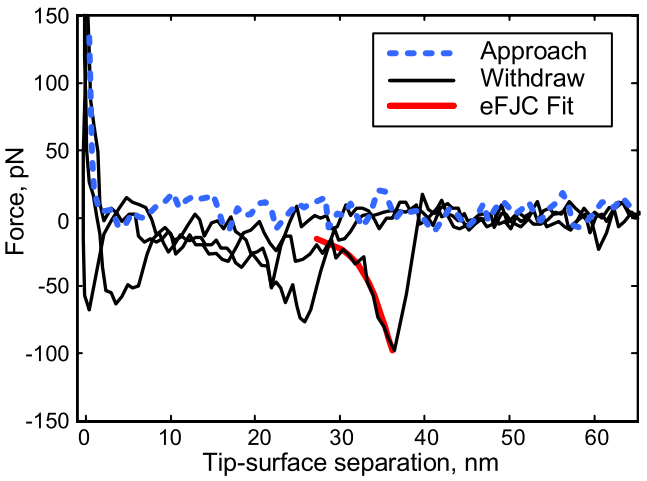

FIGURE 7 Typical force plots exhibiting the rupture events at the tip sample separation that corresponds to the tether length. Fit with the eFJC model to one of the stretching events is also included.

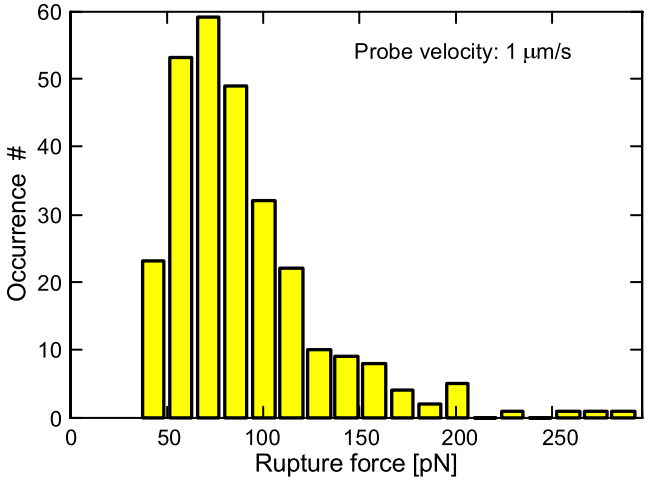

FIGURE 8 Typical distribution of rupture forces measured with 0.07 N/m probe at the probe velocity of 1002 nm/s. Biotin was attached by PEG tether with molecular mass of 3.4 kDa.

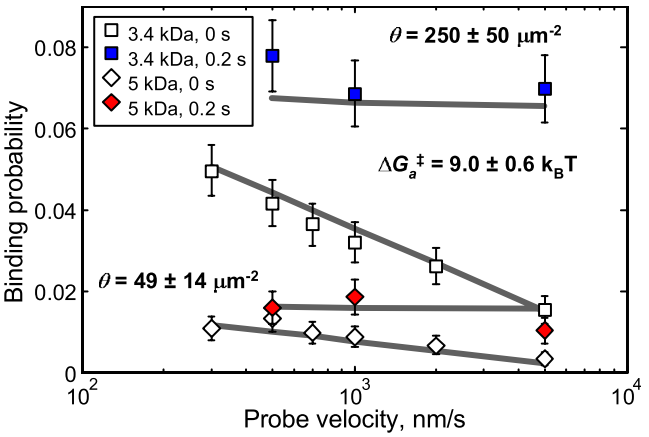

FIGURE 9 Detection probability versus AFM probe velocity (v) detected for biotin-streptavidin interaction. Biotin was tethered to the probe with 3.4 and 5 kDa PEG linkers and two different probe dwell times were used in the measurements. Lines show fits according to the model described in the text. Fit parameters of streptavidin surface coverage and activation energy of binding are shown in the graph.

For each probe velocity, we can get a rupture force distribution as shown in Fig. 8. The similarity of force plots and rupture force distributions between the current data and data obtained previously (10) indicate that these measurements are reproducible and that these measurements studied the same biotin-streptavidin interaction.

Binding probability measurements

Measured binding probabilities as a function of probe velocity are shown in Fig. 9. The measured velocity dependence is similar to the theoretical prediction shown in Fig. 2. An increase in the detection probability with an increase of the dwell time was also detected previously in measurements of other specific interactions (8,41).

All data were fit simultaneously using the FJC-based model (Eq. 9) and the modified SSS model (Eq. 12). The surface coverage for each sample and one value of the activation energy were the fit parameters; the fit procedure minimized the root mean-square error. The Kuhn length of PEG tethers was taken as 0.7 nm and the capture distance was set equal to the Kuhn length. Corresponding fit lines and fit parameters are shown in Fig. 9. Errors in parameters were calculated using a covariance matrix (42). It can be noted that the model fits the data reasonably well. The extracted $\Delta G_a^{\ddagger}$ is 9.0 ± 0.6 k_BT. If the Gaussian tether model is used the measured activation energy is 8.8 ± 0.6 k_BT. This indicates that for these data the Gaussian tether model is sufficiently accurate. To verify the consistency in the fit parameters we separately fit different subsets of the data. The fit parameters for selected data subsets are shown in Table 1. Fit parameters (including the surface grafting density) estimated from the subsets of the data fall within the limits given by the fit errors. This indicates that the activation energy and surface coverage can be estimated independently. The surface coverage was not controlled during sample preparation. Values of grafting density that we obtain are close to the range of grafting densities obtained for antibodies that were immobilized using similar amination chemistry (5). Also, the extracted values of surface coverage might be affected by contributions from the multiple rupture events and other factors that multiplicatively change binding probability. Therefore the extracted values might differ noticeably from the actual surface coverage, only providing an order of magnitude estimates.

According to the discussion above, the major contribution to the systematic error in the activation energy is the uncertainty in the attachment point of the biotin linker. Our estimates indicate that this contributes ~1 k_BT to the overestimation of the activation energy. Other sources of error (tether polydispersity, capture distance, encounter rate) contribute to the uncertainty of the measured value. Using estimates of the expected errors the corrected activation energy is $\Delta G_a^{\ddagger} = 8 \pm 1\ k_BT$.

The expected rate of association based on the measured activation energy can be compared with the association

TABLE 1 Fit parameters estimated for different subsets of the data

Data set parameters	All data $t_0 = 0$ and 0.2 s	3.4 kDa tether $t_0 = 0$ and 0.2 s	5 kDa tether $t_0 = 0$ and 0.2 s	All data $t_0 = 0$ s	3.4 kDa tether $t_0 = 0$ s	5 kDa tether $t_0 = 0$ s
$\Delta G_a^{\ddagger}$, k_BT	9.0 ± 0.6	9.3 ± 0.3	8.1 ± 1.2	8.8 ± 0.4	9.0 ± 0.2	8.4 ± 0.6
θ_1, μm^{-2}	250 ± 50	270 ± 30	—	220 ± 30	240 ± 20	—
θ_2, μm^{-2}	49 ± 14	—	38 ± 14	52 ± 10	—	45 ± 10

rate measured in solution. The expected rate can be estimated as $k' = k_S \exp(-\Delta G_a^{\ddagger}/k_BT)$, where k_S is the rate given by the Smoluchowski limit (43)

$$k_S = 4\pi(r_A + r_B)(D_A + D_B) \quad (19)$$

where r_A and r_B are the radii of interacting molecules and D_A and D_B are the corresponding diffusion coefficients. Using the Einstein-Stokes formula for the diffusion coefficients gives an estimate for $k_S \approx 10^{10}$ and $k' = 3 \pm (6,2) \times 10^6\ M^{-1}s^{-1}$. The on-rate for biotin-streptavidin interaction measured by SPR is $k_{on} = 5 \times 10^6\ M^{-1}s^{-1}$ (44). Thus, the rate of association measured with ligand freely diffusing in solution is close to the rate expected from the activation energy measured with the tethered ligand. This indicates that the effect of biotin tethering on activation energy extracted here is small (of the order of unity). However, considering that SPR might underestimate the rate of association (38) it remains possible that the actual linker effect is larger than observed here. The observed agreement is not contradictory to the large decrease known for the association constant measured in the interaction between avidin and PEGyleted biotin (45). This agreement indicates that, in the developed approach, the dynamics of the polymeric tether is adequately taken into account.

It was noted that the rate of the diffusion-controlled reactions is significantly higher than the rates expected from probabilistic models based on matching the geometries of interacting molecules (23,24,46). However, geometrical factors might be important and therefore the extracted activation energy contains a contribution from the steric factor f: $\Delta G_{exp}^{\ddagger} = \Delta G_a^{\ddagger} \times k_BT \ln(f)$ where $\Delta G_{exp}^{\ddagger}$ is the activation energy measured by the proposed method and $\Delta G_a^{\ddagger}$ is the true activation energy. The activation energy of the biotin-streptavidin association can be estimated from the thermodynamic free energy difference ΔG° and the activation free energy of dissociation $\Delta G_d^{\ddagger}$ as $\Delta G_a^{\ddagger} = \Delta G_d^{\ddagger} + \Delta G^{\circ}$ (note that ΔG° is negative and $\Delta G_d^{\ddagger}$ is positive). Using the previously reported values $\Delta G^{\circ} = 31$ and $\Delta G_d^{\ddagger} = 41 \pm 4$ (in units of thermal energy) we obtain $\Delta G_a^{\ddagger} = 10 \pm 4\ k_BT$ (11). This value is higher than the activation energy measured here by $2\ k_BT$ but remains inside of the estimated confidence region. This comparison allows the estimation of the lower bound value for the steric factor as $f_{min} = \exp(-2.2) \approx 10^{-1}$. This indicates that biotin-streptavidin association is largely limited by a reaction step. Consequently the measured activation energy corresponds to the high energy ''gate'' states (47) of the binding reaction that might have contributions from the unfavorable conformations of interacting molecules or from the solvent configurations (15,16).

CONCLUSIONS

In this study we proposed a quantitative approach to characterize the activation energy of association in bimolecular reactions by measuring dependence of the binding probability on AFM probe velocity. The developed approach takes into account tether dynamics and extracts activation energy of association as if there were no polymeric tether attached to the ligand. We have considered different sources of error and concluded that results of this method are reasonably accurate (with ~1 k_BT error). In combination with the more traditional force spectroscopy analysis of rupture forces this new (to our knowledge) method provides kinetic parameters of association and dissociation from a single experiment. This method has several advantages in comparison to the established biosensor-based techniques: detection is based on measurements of interaction forces thus directly probing interactions understudy; this approach alleviates problems of biosensor methods associated with high grafting density of interacting molecules and the mass-transport limitations; and this approach can also be used to study interactions locally. Further, comparing results of this single-molecule technique to temperature-based measurements of activation energy can be used to quantify the steric factors of the molecular interaction.

The developed approach was applied to study interactions between biotin and streptavidin. The measured activation energy is consistent with SPR results, indicating that dynamics of polymeric tether is adequately taken into account. Comparison with the activation free energy derived from temperature measurements of the dissociation rate between biotin and streptavidin indicate that the steric factor is high (>~0.1) and that binding is limited by the reaction step.

The described approach can be adopted to study other bimolecular reactions that have high activation barrier to dissociation (this is necessary because the detection is based on detection of rupture events). The local detection character of this technique is attractive in quantifying the activation energy and approximate surface coverage at heterogeneous biological surfaces. Because approach presented here requires low grafting density (in comparison to the biosensor methods like SPR), it might provide an interesting way to test the contribution of the ligand surface diffusion (reduction-of-dimensionality) on kinetics of association (48).

This work was supported by Duke University, the National Science Foundation (grant CHE-0719043), the Army Research Office (W911NF-04-100191), and Gilbert Walker.

REFERENCES

1. Evans, E., and K. Ritchie. 1997. Dynamic strength of molecular adhesion bonds. *Biophys. J.* 72:1541–1555.
2. Dudko, O. K., G. Hummer, and A. Szabo. 2006. Intrinsic rates and activation free energies from single-molecule pulling experiments. *Phys. Rev. Lett.* 96:108101–108104.
3. Ray, C., J. R. Brown, A. Kirkpatrick, and B. B. Akhremitchev. 2008. Pairwise interactions between linear alkanes in water measured by AFM force spectroscopy. *J. Am. Chem. Soc.* 130:10008–10018.
4. Friddle, R. W., P. Podsiadlo, A. B. Artyukhin, and A. Noy. 2008. Near-equilibrium chemical force microscopy. *J. Phys. Chem. C.* 112: 4986–4990.

5. Hinterdorfer, P., W. Baumgartner, H. J. Gruber, K. Schilcher, and H. Schindler. 1996. Detection and localization of individual antibody-antigen recognition events by atomic force microscopy. *Proc. Natl. Acad. Sci. USA*. 93:3477–3481.
6. Kuhner, F., and H. E. Gaub. 2006. Modelling cantilever-based force spectroscopy with polymers. *Polymer (Guildf.)*. 47:2555–2563.
7. Ray, C., and B. B. Akhremitchev. 2005. Conformational heterogeneity of surface-grafted amyloidogenic fragments of alpha-synuclein dimers detected by atomic force microscopy. *J. Am. Chem. Soc.* 127:14739–14744.
8. Baumgartner, W., P. Hinterdorfer, W. Ness, A. Raab, D. Vestweber, et al. 2000. Cadherin interaction probed by atomic force microscopy. *Proc. Natl. Acad. Sci. USA*. 97:4005–4010.
9. Jeppesen, C., J. Y. Wong, T. L. Kuhl, J. N. Israelachvili, N. Mullah, et al. 2001. Impact of polymer tether length on multiple ligand-receptor bond formation. *Science*. 293:465–468.
10. Guo, S., C. Ray, A. Kirkpatrick, N. Lad, and B. B. Akhremitchev. 2008. Effects of multiple-bond ruptures on kinetic parameters extracted from force spectroscopy measurements: revisiting biotin-streptavidin interactions. *Biophys. J.* 95:3964–3976.
11. Chilkoti, A., and P. S. Stayton. 1995. Molecular-origins of the slow streptavidin-biotin dissociation kinetics. *J. Am. Chem. Soc.* 117:10622–10628.
12. Grubmuller, H., B. Heymann, and P. Tavan. 1996. Ligand binding: molecular mechanics calculation of the streptavidin biotin rupture force. *Science*. 271:997–999.
13. Izrailev, S., S. Stepaniants, M. Balsera, Y. Oono, and K. Schulten. 1997. Molecular dynamics study of unbinding of the avidin-biotin complex. *Biophys. J.* 72:1568–1581.
14. Merkel, R., P. Nassoy, A. Leung, K. Ritchie, and E. Evans. 1999. Energy landscapes of receptor-ligand bonds explored with dynamic force spectroscopy. *Nature*. 397:50–53.
15. Stayton, P. S., S. Freitag, L. A. Klumb, A. Chilkoti, V. Chu, et al. 1999. Streptavidin-biotin binding energetics. *Biomol. Eng.* 16:39–44.
16. Young, T., R. Abel, B. Kim, B. J. Berne, and R. A. Friesner. 2007. Motifs for molecular recognition exploiting hydrophobic enclosure in protein-ligand binding. *Proc. Natl. Acad. Sci. USA*. 104:808–813.
17. Szabo, A., K. Schulten, and Z. Schulten. 1980. First passage time approach to diffusion controlled reactions. *J. Chem. Phys.* 72:4350–4357.
18. Shoup, D., and A. Szabo. 1982. Role of diffusion in ligand-binding to macromolecules and cell-bound receptors. *Biophys. J.* 40:33–39.
19. Northrup, S. H., S. A. Allison, and J. A. McCammon. 1984. Brownian Dynamics simulation of diffusion-influenced bimolecular reactions. *J. Chem. Phys.* 80:1517–1526.
20. Berne, B. J., M. Borkovec, and J. E. Straub. 1988. Classical and modern methods in reaction-rate theory. *J. Phys. Chem.* 92:3711–3725.
21. Oesterhelt, F., M. Rief, and H. E. Gaub. 1999. Single molecule force spectroscopy by AFM indicates helical structure of poly(ethyleneglycol) in water. *New J. Phys.* 1:6.1–6.11.
22. Krasnoslobodtsev, A. V., L. S. Shlyakhtenko, and Y. L. Lyubchenko. 2007. Probing interactions within the synaptic DNA-Sfil complex by AFM force spectroscopy. *J. Mol. Biol.* 365:1407–1416.
23. Shoup, D., G. Lipari, and A. Szabo. 1981. Diffusion-controlled bimolecular reaction rates. The effect of rotational diffusion and orientation constraints. *Biophys. J.* 36:697–714.
24. Schlosshauer, M., and D. Baker. 2004. Realistic protein-protein association rates from a simple diffusional model neglecting long-range interactions, free energy barriers, and landscape ruggedness. *Protein Sci.* 13:1660–1669.
25. Toan, N. M., G. Morrison, C. Hyeon, and D. Thirumalai. 2008. Kinetics of loop formation in polymer chains. *J. Phys. Chem. B*. 112:6094–6106.
26. Pastor, R. W., R. Zwanzig, and A. Szabo. 1996. Diffusion limited first contact of the ends of a polymer: Comparison of theory with simulation. *J. Chem. Phys.* 105:3878–3882.
27. Gu, C., A. Kirkpatrick, C. Ray, S. Guo, and B. B. Akhremitchev. 2008. Effects of multiple-bond ruptures in force spectroscopy measurements of interactions between Fullerene C60 molecules in water. *J. Phys. Chem. C*. 112:5085–5092.
28. Sulchek, T., R. W. Friddle, and A. Noy. 2006. Strength of multiple parallel biological bonds. *Biophys. J.* 90:4686–4691.
29. Ratto, T. V., R. E. Rudd, K. C. Langry, R. L. Balhorn, and M. W. McElfresh. 2006. Nonlinearly additive forces in multivalent ligand binding to a single protein revealed with force spectroscopy. *Langmuir*. 22:1749–1757.
30. Zlatanova, J., S. M. Lindsay, and S. H. Leuba. 2000. Single molecule force spectroscopy in biology using the atomic force microscope. *Prog. Biophys. Mol. Biol.* 74:37–61.
31. Hanley, W., O. McCarty, S. Jadhav, Y. Tseng, D. Wirtz, et al. 2003. Single molecule characterization of P-selectin/ligand binding. *J. Biol. Chem.* 278:10556–10561.
32. Kienberger, F., A. Ebner, H. J. Gruber, and P. Hinterdorfer. 2006. Molecular recognition imaging and force spectroscopy of single biomolecules. *Acc. Chem. Res.* 39:29–36.
33. Sarid, D. 1994. Scanning Force Microscopy. Oxford University Press, New York.
34. Viani, M. B., T. E. Schaffer, A. Chand, M. Rief, H. E. Gaub, et al. 1999. Small cantilevers for force spectroscopy of single molecules. *J. Appl. Phys.* 86:2258–2262.
35. Ray, C., J. R. Brown, and B. B. Akhremitchev. 2007. Rupture force analysis and the associated systematic errors in force spectroscopy by AFM. *Langmuir*. 23:6076–6083.
36. Ratto, T. V., K. C. Langry, R. E. Rudd, R. L. Balhorn, M. J. Allen, et al. 2004. Force spectroscopy of the double-tethered concanavalin-A mannose bond. *Biophys. J.* 86:2430–2437.
37. Averett, L. E., C. B. Geer, R. R. Fuierer, B. B. Akhremitchev, O. V. Gorkun, et al. 2008. Complexity of ''A-a'' knob-hole fibrin interaction revealed by atomic force spectroscopy. *Langmuir*. 24:4979–4988.
38. Schuck, P. 1997. Use of surface plasmon resonance to probe the equilibrium and dynamic aspects of interactions between biological macromolecules. *Annu. Rev. Biophys. Biomol. Struct.* 26:541–566.
39. Hyre, D. E., L. M. Amon, J. E. Penzotti, I. Le Trong, R. E. Stenkamp, et al. 2002. Early mechanistic events in biotin dissociation from streptavidin. *Nat. Struct. Biol.* 9:582–585.
40. Ramsden, J. J. 1997. Optical biosensors. *J. Mol. Recognit.* 10:109–120.
41. Gilbert, Y., M. Deghorain, L. Wang, B. Xu, P. D. Pollheimer, et al. 2007. Single-molecule force spectroscopy and imaging of the vancomycin/D-Ala-D-Ala interaction. *Nano Lett.* 7:796–801.
42. Bevington, P. R., and D. K. Robinson. 2003. Data Reduction and Error Analysis for the Physical Sciences. McGraw-Hill, New York.
43. Berg, O. G., and P. H. Vonhippel. 1985. Diffusion-controlled macromolecular interactions. *Annu. Rev. Biophys. Biophys. Chem.* 14:131–160.
44. Qureshi, M. H., J. C. Yeung, S.-C. Wu, and S.-L. Wong. 2001. Development and characterization of a series of soluble tetrameric and monomeric streptavidin muteins with differential biotin binding affinities. *J. Biol. Chem.* 276:46422–46428.
45. Ke, S., J. C. Wright, and G. S. Kwon. 2007. Intermolecular interaction of avidin and PEGylated biotin. *Bioconjug. Chem.* 18:2109–2114.
46. Northrup, S. H., and H. P. Erickson. 1992. Kinetics of protein protein association explained by Brownian dynamics computer-simulation. *Proc. Natl. Acad. Sci. USA*. 89:3338–3342.
47. Zhou, H. X., and A. Szabo. 1996. Theory and simulation of stochastically-gated diffusion-influenced reactions. *J. Phys. Chem.* 100:2597–2604.
48. Axelrod, D., and M. D. Wang. 1994. Reduction-of-dimensionality kinetics at reaction-limited cell-surface receptors. *Biophys. J.* 66: 588–600.